



Finite element modeling of heat transfer in pulsed laser welding of similar and dissimilar carbon and stainless steels

Zohre Tajbakhshjoo, Eslam Ranjbarnodeh*, Ali Farzadi 

Department of Materials and Metallurgical Engineering, Amirkabir University of Technology (Tehran Polytechnic), Tehran, Iran

ABSTRACT: Laser welding is one of the most prominent manufacturing methods in various industries due to its speed and high quality. The laser beam welding process has two modes of conduction and keyhole. The keyhole mode is more attractive due to its greater penetration depth and smaller heat-affected zone. To achieve the keyhole mode, it is necessary to adjust the welding process variables, which requires many experiments. Hence, simulation can be used as a powerful tool to reduce the cost. In this study, similar and dissimilar lap joints of low-carbon steel and stainless steel using pulsed laser welding were simulated by finite element software ANSYS. The effects of pulse energy and frequency were examined and the values for obtaining the keyhole mode were determined. Simulated weld pool dimensions were compared to experimental results and the good agreement between them showed that the model is appropriate for simulating pulsed laser welding. Numerical results showed that the keyhole mode is created in dissimilar joints of low-carbon steel and stainless steel, similar joints of stainless steel, and similar joints of low-carbon steel at pulse energies of 17.1, 11.8, and 13.9 J, respectively. A pulse frequency of 14 Hz was found to be the optimal condition for the formation of the keyhole.

Review History:

Received: Sep. 11, 2022

Revised: Feb. 15, 2023

Accepted: Jun. 18, 2023

Available Online: Jul. 04, 2023

Keywords:

Pulse frequency

Pulse energy

Simulation

Lap joint

Penetration depth

1- Introduction

Laser welding is one of the most widely used joining processes in various industries such as shipbuilding, automotive, and electronics. The unique advantages of this process versus other conventional welding processes are a high power density heat source, deep penetration of the weld, high ratio of weld depth to width, and narrow heat-affected zone [1]. Also, the slight losses in the laser process have turned it into a cost-effective way to make joints in structures where stainless steel is used [2].

In the past decades, researchers have used analytical methods and finite element simulations to predict the temperature, residual stress, and distortion induced by laser beam welding. Rosenthal [3] modeled laser welding with a spot heat source. Frewin and Scott [4] simulated the pulsed laser-induced heat flow with a 3D finite element method. Mahrle and Schmidt [5] presented a mathematical model for the simulation of a weld pool with high penetration depth and explored the effect of fluid flow in the welding zone. Tsirkas et al. [6] used finite element software (SYSWELD) to examine laser welding on marine steel and addressed the thermal, metallurgical, and mechanical effects. Sunar et al. [7] employed the finite element software ANSYS to calculate stresses in the welding zone. Sabbaghzadeh et al. [8] used a finite element model and finite difference method

for thermal simulation of laser welding. They obtained transient temperature profile, welding pool dimensions, and heat-affected zone in stainless steel 304 and revealed that penetration depth and heat profile strongly depended on the pulse parameters of the laser. Yilbas et al. [9] simulated laser welding in low-carbon steel and verified the estimated stresses by the XRD method. In another study, the variables optimized for achieving full penetration depth were obtained by SYSWELD and were compared with experimental results [10]. Shanmugam et al. [11] used ANSYS to simulate weld shape in the laser spot welding process. In the simulation, they used a conical Gaussian heat source for thermal modeling and compared the results with experimentations on AISI 304 steel.

Laser beam welding may, however, use pulsed or continuous lasers depending on the welding type. When small spot welds are required, single pulses of the laser may suffice. But, in the case of continuous welding, a steady laser beam is used. In pulsed laser welding, the weldment is continuously heated by short pulses up to temperatures above the melting temperature. The melted points may overlap or be separated depending on the welding speed [12]. In a study on the response of materials to pulsed wave and continuous wave laser welding under similar conditions (similar power density, interaction time, and beam diameter), it was found that the pulsed wave welding exhibited deeper penetration. This deeper penetration of pulsed wave, versus continuous wave,

*Corresponding author's email: islam_ranjbar@aut.ac.ir



results in a much lower input heat requirement to reach the same penetration depth [13]. Pulsed wave laser welding has further advantages over continuous wave welding, including less distortion and its capability to weld heat-sensitive compounds. Much of the research on laser welding has been conducted on stainless steel because of the vital significance of stainless steel in power plants and chemical industries [14, 15]. A new mass application of this weld is in manufacturing tailor-welded blanks for the automobile body [14]. Sun et al. [15] studied the weldability of different metals and concluded that laser welding can be exercised on austenitic stainless steel unless those that are prone to solidification crack due to their high sulfur content. Berretta et al. [16] explored the welding of AISI 304 to AISI 420 stainless steels and examined the effect of the laser beam position with respect to the joint on the weld properties. Another issue to consider in laser beam welding is the dissimilar joint of stainless steel to low-carbon steel. This kind of joint is widely used in pressure vessels, boilers, and heat exchangers in the power industry and petrochemical plants [17]. The different physical and chemical characteristics of the two base metals cause the weld metal can behave significantly differently from one or both parent metals in service.

Therefore, it is a key requirement for laser-aided joints to select suitable welding variables to accomplish optimal microstructure and mechanical properties [2, 10]. Aghaee et al. [18] investigated the temperature and strain distribution in dissimilar welding between Copper and 304 stainless steel. Their results showed that Cu has a narrower HAZ in comparison to stainless steel. Mohammadpour et al. [19] studied the effect of dual laser beams on dissimilar welding-brazing of aluminum to galvanized steel. Their results showed that a dual-beam laser shape and high scanning speed could control the thickness of the intermetallic and alter the failure location of the joint. Jiang et al. [20] predicted thermal cycles during single-pass laser welding of 20 mm-thick high-strength steel under reduced ambient pressure and compared the calculated results to experiments. They showed that the weld pool had a lower peak temperature under reduced ambient pressure.

One of the most prominent features of laser welding is the ability to create a pool in the form of a keyhole. This mode of laser welding increases the depth of penetration and reduces the size of the heat-affected zone. To achieve the keyhole mode, it is essential to adjust the welding process variables. Achieving this goal only with experimental tests is time-consuming and costly. To save these resources, finite element simulation is an effective method. Yan et al. [21] used (FE) analysis to predict the effect of oscillation parameters on the temperature field and residual stress and as-welded distortion of 316 LN stainless steel weld joint. Uni et al. [22] use computational fluid dynamics to model heat transfer, and weld pool flow during keyhole laser welding of 316 LN stainless steel using a hybrid conical-cylindrical heat source. They showed that this hybrid heat source model is very useful for predicting transfer phenomena in this type of welding.

Achieving a suitable penetration depth in the welding processes is constantly challenging. In laser beam welding, the penetration depth can be dramatically increased by keyhole mode. Hence, the effects of pulse frequency and pulse energy on weld pool geometry were modeled in this manuscript. The values of pulse frequency and pulse energy for obtaining the keyhole mode were determined in similar and dissimilar joints of carbon and stainless steel. These values are applicable to engineers and scientists. Simulations were validated by comparing them with experiments. The dissimilar joint, lap joint design, pulsed welding process, verifications, and precision of results are the most important scientific innovations. It is worth note that there are few studies on the combination of lap joint and pulse laser welding process.

2- Model

Here, the experimental results and data of Massoomi and Sepasi [23] were used to verify the numerical results. Hence, the experimental steps are first reviewed briefly. In the experimental work, two plates of uncoated low-carbon steel and 304L austenitic stainless steel with a thickness of 0.8 mm were used as the base metals. In that study, the welding was performed by an IQL-10 pulsed Nd: YAG laser source with an average maximum power of 400 W. The mentioned laser source can produce square pulses with a width of 0.2-20 ms and a frequency of 1000 Hz with a maximum energy of 40 J. The focusing optical system consists of three lenses with a 75-mm focal length. Optical adjustments were made so that the diameter of the laser beam on the workpiece was about 300 μm . The lap joint design was used and a circular welding path was applied as depicted in Fig. 1. Thereby, a welding ring was created that was geometrically analogous to the weld nugget in resistance spot welds. The dimensions of the welded sample are selected so that after welding it is subjected to a tensile-shear test [23]. To reasonably simplify the finite element simulation of laser welding in a lap joint configuration, some basic assumptions have been applied. First, the fluid flow in the molten pool was ignored and the surface of the pool was assumed to be flat. The next assumption is that changes in material properties due to phase transformation during cooling (for carbon steel) were ignored. The first step to start the analyses was the modeling of the geometry and meshing of the joint. Since in the present study, the two plates were overlapped and the laser beam was applied from the upper surface to the desired point, the accuracy of the meshing was of high importance. Due to the generation of a high thermal gradient in the zones near the welding line, the meshing should be finer. Also, to reduce the calculation time, the meshing should be bigger at points that were more distant from the welding line. Fig. 2 displays a schematic of the built model and its elements. In this model, the Solid70 element was used for bulk meshing and the Surf152 surface elements were used on the top surface to apply the boundary condition (heat source) on the surfaces. The model was composed of a total of 75,751 nodes and 45,568 elements.

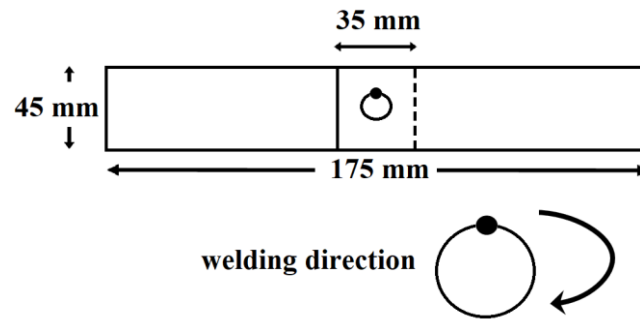


Fig. 1. The dimensions and design of the joint in the experimental work [20]

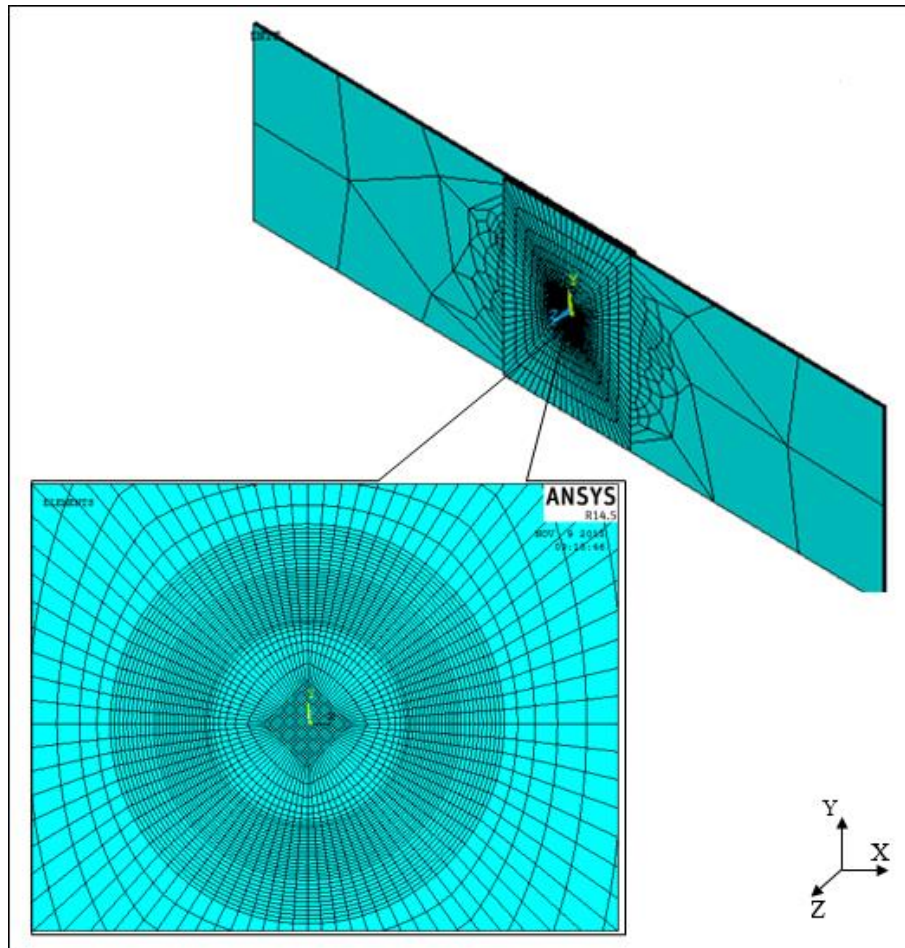


Fig. 2. The used model and meshing

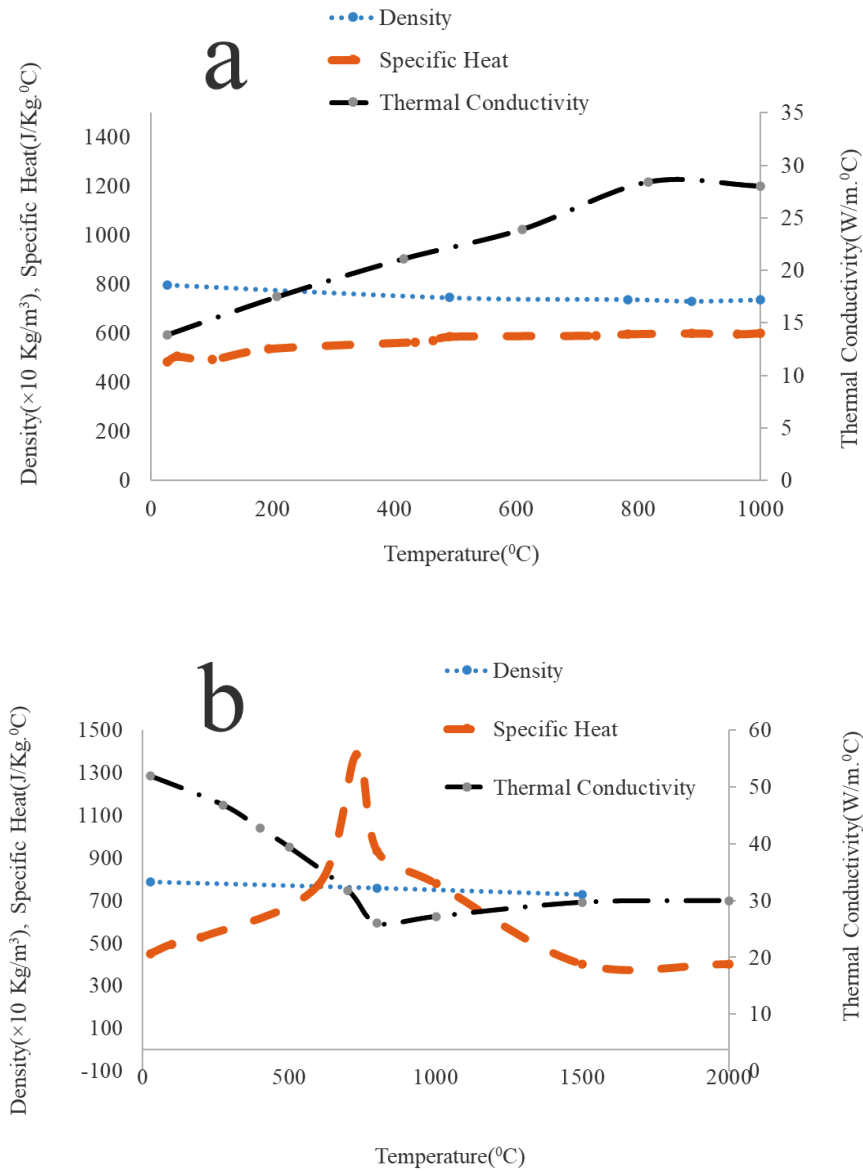


Fig. 3. (a) The thermal properties of the stainless steel; (b) the thermal properties of the low-carbon steel [21, 22]

Because in the welding process, the temperature of the welded specimen changes drastically, the material properties are assumed to be temperature-dependent in the simulation. To account for the heat transfer by turbulence and fluid flow inside the weld pool, the coefficient of thermal conductivity was multiplied by 3 at temperatures above the melting point, which is 1500°C for low-carbon steel and 1400°C for stainless steel [5]. Fig. 3 displays the thermal properties of stainless steel [24] and low-carbon steel [25].

Considering the nature of the laser beam welding process, a model is desirable that considers the keyhole phenomenon and has a correct volume distribution of energy along the material thickness. Various models have been developed

for this type of welding for the heat source, among which the hybrid models are very accurate and provide a good description of the shape of the keyhole. Hence, this study used a hybrid model consisting of a planar heat source on the top surface and a conical heat source through the thickness of the base metals [11, 26, 27]. The Eq. (1) used to express the heat distribution across the surface is as below:

$$Q(x, y) = \frac{3Q_{surf}}{\pi R^2} \cdot \exp\left(-\frac{3(x^2 + y^2)}{R^2}\right) \quad (1)$$

Table 1. The variables used in examining the effect of the pulse energy on the weld pool dimensions

Joint type	Welding variables				Welded ring diameter (mm)
	Pulse energy	Pulse width	Repetition frequency	Welding speed	
	(J)	(ms)	(Hz)	(mm/s)	
Low-carbon	12.9, 13.9, 15,	8.5	14	3	6
to stainless steel	16.1, 17, 18, 19.3				

where R is the radius of the heat source, which is obtained by using the focal length of the condenser lens and Eq. (2) as below [11]:

$$R = \frac{2M_0^2 \lambda F}{\pi D_0^2} \quad (2)$$

where M_0^2 is the beam quality (it is 1.04 for an Nd:YAG lens with $\lambda = 1.06 \mu\text{m}$), F is the focal distance from condenser lens (75 mm), and D_0 is the minimum diameter of the laser beam (6 mm is the set parameter of the machine during welding). The conical model is also as a Gaussian distribution on the x-y plane and a linear distribution along the depth (z) and is defined by Eq. (3) as below:

$$q(x, y, z) = \frac{6Q_{keyhole}}{a_c b_c c_c \pi^{1.5}} \exp\left(-3\frac{x^2}{a_c^2}\right) \times \left[1 - \frac{(1-d_c) \cdot |z|}{b_c}\right] \exp\left(-3\frac{y^2}{c_c^2}\right) \quad (3)$$

where a_c , b_c , and c_c are the variables related to the cone. In the conical model, the linear decrease in energy intensity along the depth is controlled by the variable d_c , which ranges from 1 to 0. If $d_c = 1$, the energy intensity at depth is constant along the parallel line of the z-axis, but if $d_c = 0$, the energy intensity decreases linearly and becomes zero at the depth b_c . The variable b_c is usually considered equal to the thickness of the weldment. Since most heat is transferred by radiation or convection in laser beam welding, these boundary conditions must be applied for simulation. However, it should be noted that, according to reports on laser welding, the fraction of the energy that is lost by reflection accounts for 30 percent, and 70 percent of the laser energy is absorbed [11, 28, 29]. Thus, the amount of energy absorption in simulations can be replaced for applying the boundary condition of the radiation. But we applied the radiation boundary condition here using

temperature-dependent properties as well as the Surf152 element on the top surface. The convective heat transfer coefficient was assumed to be 15 W/m²K at all levels except for the bottom surface, which was considered 1000 W/m²K. First, the heat source variables were calibrated according to the welding process and then the welding analysis was performed. Finally, the influences of welding variables such as pulse energy, frequency were analyzed on the dimensions of weld pool according to Tables 1-3.

3- Results and Discussion

Figs. 4 and 5 display the temperature distribution across the cross-sectional area of a similar joint of low-carbon steel and stainless steel at a pulse energy of 15 J, a frequency of 14 Hz, a welding speed of 3 mm/s, and a pulse width of 8.5 ms, 0.2 seconds after the onset of welding, respectively. As can be seen, the highest temperature is related to the center line of the weld, which temperature has reached 2166 °C for a similar joint of carbon steel and 2144 °C for stainless steel. Stainless steel experiences a higher temperature at the same heat input due to less thermal diffusivity. Similar behavior has been reported by other researchers [18]. Fig. 6 shows the dissimilar lap joint between stainless and carbon steel.

In the next step, the study was focused on investigating the effect of the pulse energy on weld pool dimensions. Fig. 7 shows the cross-sectional area variations of laser spot welds in the experimental and simulated state of the similar joints of the low-carbon steel at pulse energies of 13.9, 15, and 18.2 J. In this case, the simulation error is less than 10%, indicating a good agreement between the results of the FEM and the experimental work. The criterion to create a keyhole mode is the width/depth ratio to be <1. According to Fig. 8, this mode is provided for a similar joint of low-carbon steel at a pulse energy of 13.9 J. Fig. 8 demonstrates the macro images and the results of the cross-sectional simulation of laser spot welds for stainless steel joints at pulse energies of 13.9, 15, and 18.2 J, which illustrate how the shape and size of the melt zone change with the increase in the laser pulse energy. As the laser pulse energy increases, the size of the weld pool increases.

The comparison of the results of the experiments and

Table 2. The variables used in examining the effect of the frequency on the weld pool dimensions

Joint type	Welding variables				Welded ring diameter (mm)
	Pulse energy (J)	Pulse width (ms)	Repetition frequency (Hz)	Welding speed (mm/s)	
	Similar and dissimilar joint of low-carbon steel to stainless steel	12.9	8.5	10, 12, 14, 15, 16	

Table 3. The variables used in examining the effect of the pulse width on the weld pool dimensions

Joint type	Welding variables				Welded ring diameter (mm)
	Pulse energy (J)	Pulse width (ms)	Repetition frequency (Hz)	Welding speed (mm/s)	
	Low-carbon to stainless steel	12.9	8.5	14	

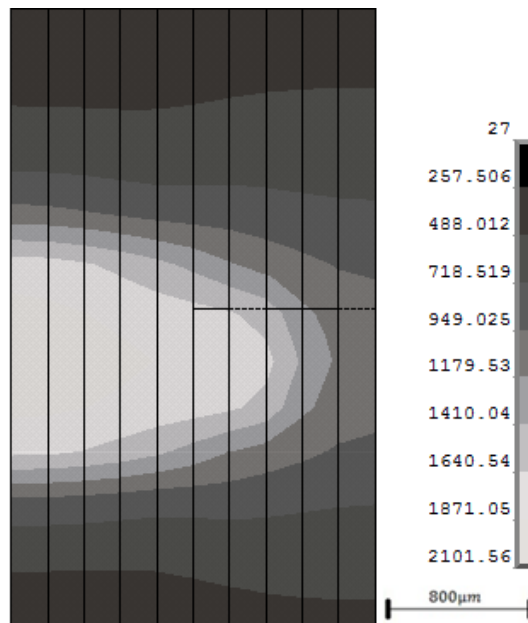


Fig. 4. The temperature distribution across the cross-section of a similar joint of low-carbon steel at a pulse energy of 15 J and a frequency of 14 Hz

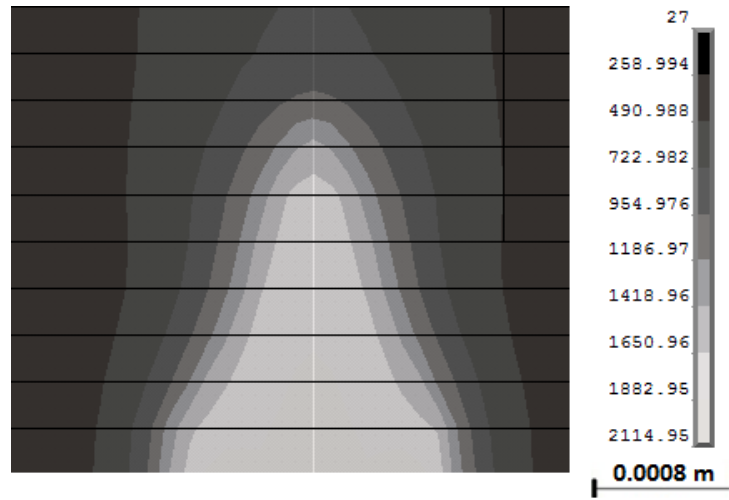


Fig. 5. The temperature distribution across the cross-section of similar joints of stainless steel at a pulse energy of 15 J and a frequency of 14 Hz

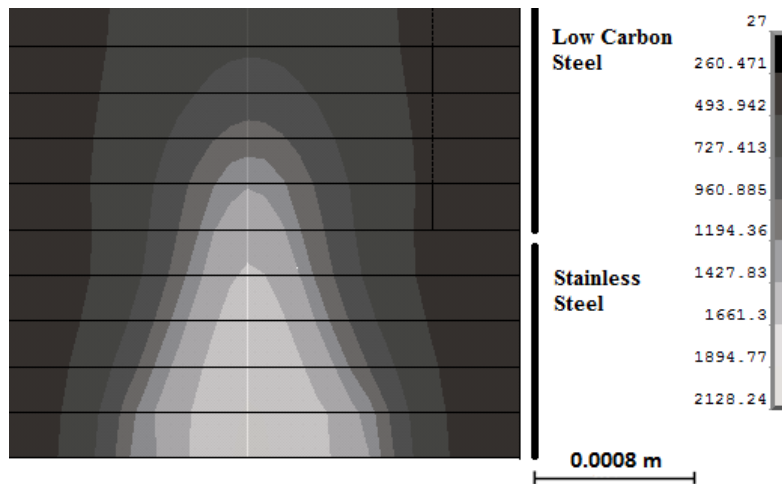


Fig. 6. The temperature distribution across the cross-section of dissimilar joint of stainless steel to low-carbon steel at pulse energy of 15 J and a frequency of 14 Hz

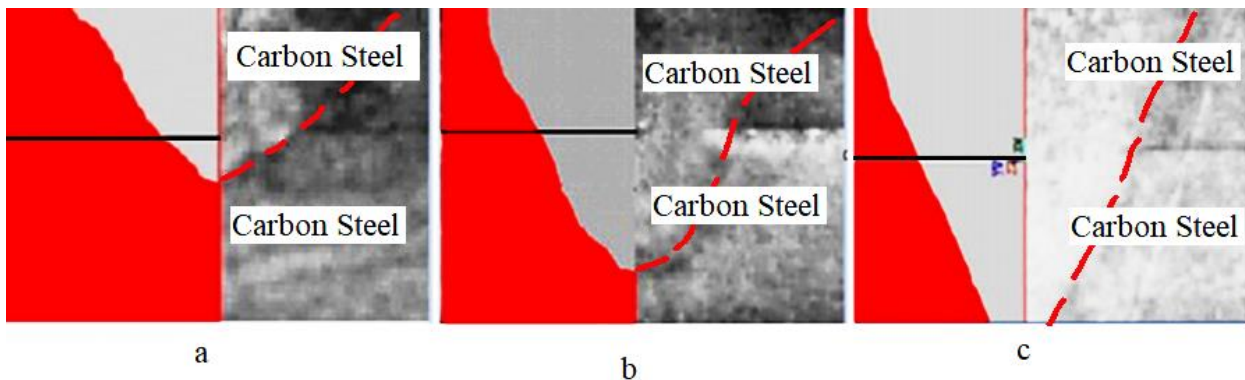


Fig. 7. The development of the weld pool size with the increase in the laser pulse energy in the similar joint of low-carbon steel – (a) 13.9 J, (b) 15 J, and (c) 18.2 J

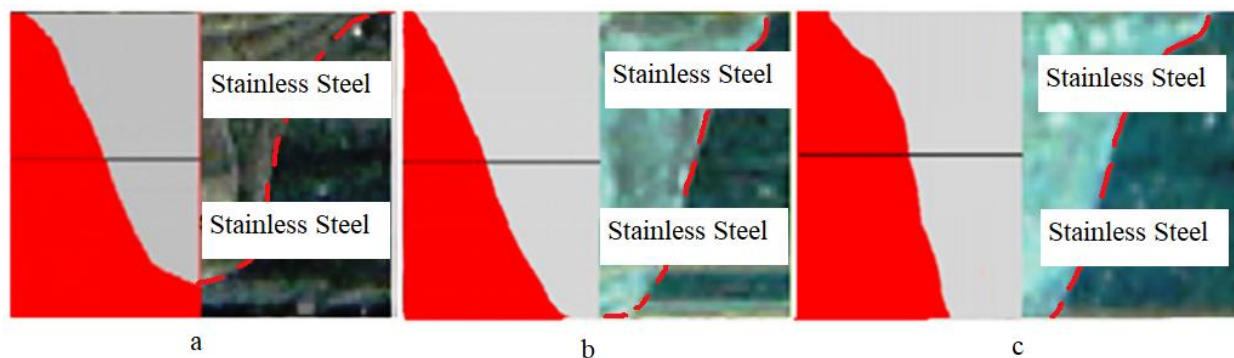


Fig. 8. The development of the weld pool size with the increase in the laser pulse energy in the similar joint of stainless steel – (a) 13.9 J, (b) 15 J, and (c) 18.2 J

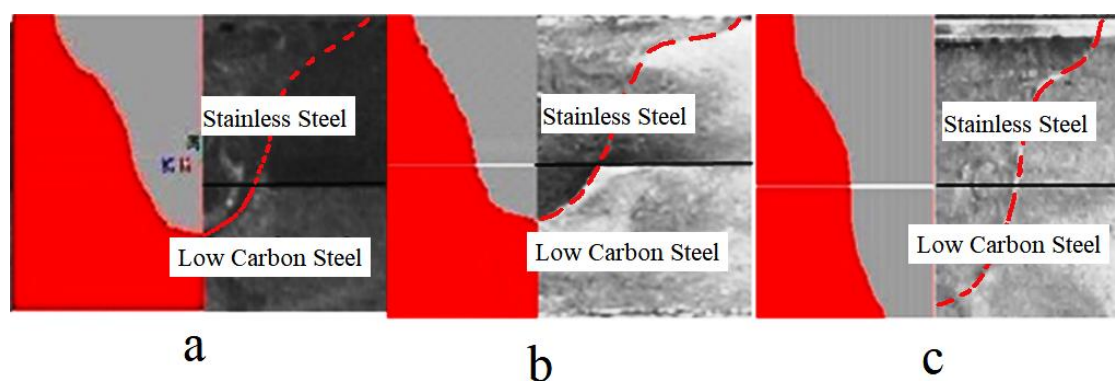


Fig. 9. The development of the weld pool size with the increase in the laser pulse energy in the dissimilar joint – (a) 13.9 J, (b) 15 J, and (c) 17.1 J

the simulation results for the dissimilar joint of low-carbon steel to stainless steel is presented in Fig. 9. This figure shows a reasonable agreement between the simulation and experimental results so that the weld dimension error is 4-8% in the width and depth. The figure shows that with the increase in pulse energy, the width of the weld pool increases. In dissimilar joints, in addition to the single-side nature of the laser beam welding process, the difference in laser absorption and thermal properties of low-carbon and austenitic stainless steel results in differences in heat transfer in these two materials. This may, in turn, influence the formation and growth of the weld metal. Lower thermal diffusivity of austenitic stainless steel than that of low-carbon steel causes the melt zone to be greater in the former than in the latter. As the figure shows, the keyhole mode for the dissimilar joint is obtained at a pulse energy of 17.1 J.

Fig. 10 depicts the variations of the weld pool dimensions with the laser pulse energy in a similar joint of low-carbon steel. It is observed that in general, as the laser pulse energy increases, the weld penetration and joint width are increased. The results show that initially as the pulse energy is increased

from 12.9 to 13.9 J, the weld penetration gradually increases. As the pulse energy increases further, the rate of increase in penetration is escalated. Seemingly, a keyhole (the depth-to-width ratio of the weld pool is above 1.5) is formed in the bottom plate as the pulse energy is increased from 13.9 to 18.2 J. After the keyhole is formed, the penetration depth gradually increases until the 18.2 J pulse energy in which almost the full penetration is achieved. After reaching full penetration, the further increase in the pulse energy does not have much effect on the dimensions of the weld pool because the laser beam is fully penetrative through the sheet thickness.

Fig. 11 depicts variations of the weld pool dimensions in the similar joint of the stainless steel in terms of laser pulse energy. It is observed that as the laser pulse energy increases, the weld penetration and joint width are increased. As the pulse energy changes from 11.8 to 15 J, the weld dimensions, especially the depth of penetration, increase dramatically. At this pulse energy, a keyhole is formed at the bottom plate. The reason for this increase in the dimensions of the weld pool with the increase in pulse energy is the increase in the amount of heat input to the base metal. After reaching a limit value,

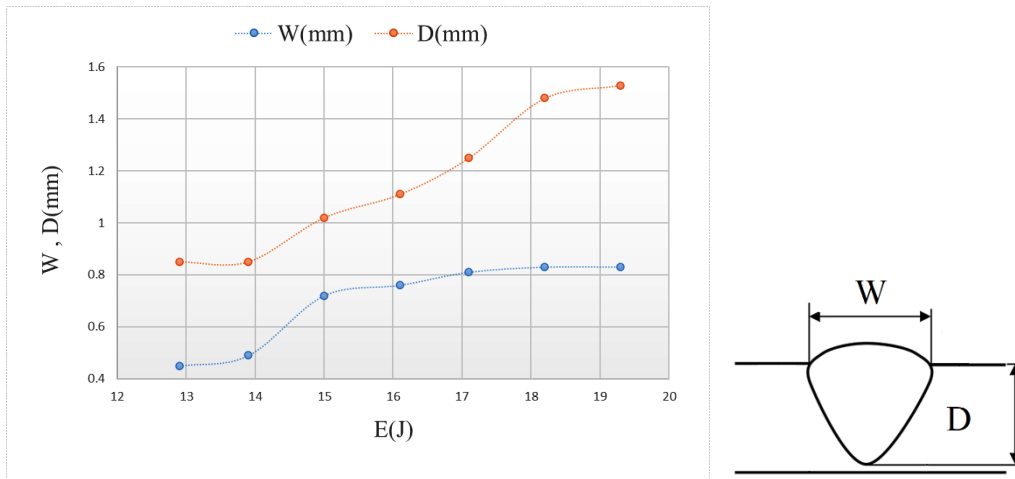


Fig. 10. The effect of pulse energy on weld pool dimensions ratio in the similar joint of low-carbon steel

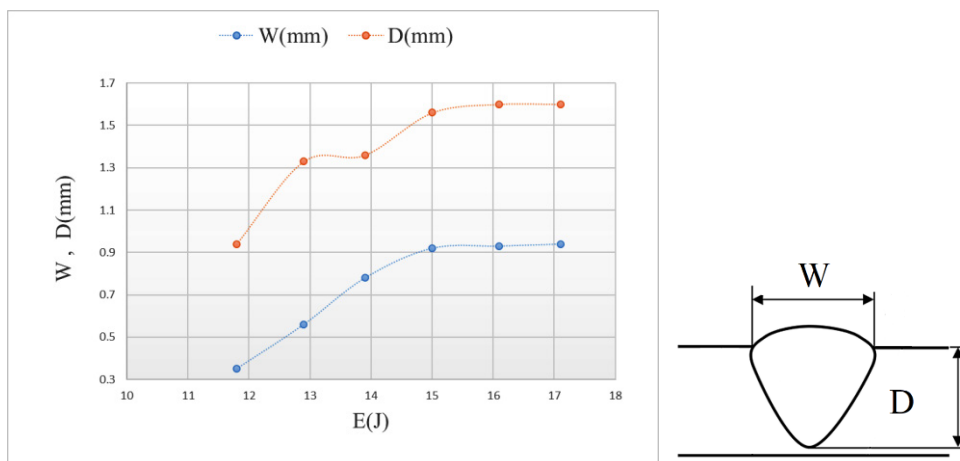


Fig. 11. The effect of pulse energy on weld pool dimensions in the similar joint of stainless steel

the rate of this increase decreases, which is due to the increase in temperature and the resulting thermal gradient compared to the areas around the weld. This gradient increases the rate of heat transfer to the surroundings and less heat is used to form the pool. According to Fig. 8, at the pulse energy of 15 J, a complete penetration happens in the thickness of two overlapped plates. After reaching the full penetration the further increase in pulse energy does not influence the melt zone dimensions significantly because the laser beam is fully penetrative through the sheet thickness.

Fig. 12 shows variations of the weld pool dimensions in the dissimilar joint of low-carbon steel to stainless steel with the increase in the pulse energy from 11.9 to 19.3 J in the simulated and experimental laser modes. The curve indicates an increase in the size of the melted zone with an increase in heat input. It is evident in Fig. 12 that, in all specimens, a

keyhole is formed in the upper plate and the weld penetrates the thickness of the upper plate. As the pulse energy is increased from 15 to 17.1 J, a sharp rise is observed in the welding penetration, which is attributed to the formation of the keyhole in the low-carbon steel plate. With the formation of a keyhole, the absorption rate of the radiation increases dramatically. In fact, it is as if there is an energy source inside the keyhole that causes much of the energy to be absorbed and melt the metal. This increases the penetration depth of the melted zone significantly and increases the depth/width ratio of the weld metal. At the pulse energy of 17.1 J, the penetration is complete beyond which no significant changes happen in the pool dimensions with a further increase in the pulse energy.

To assess the effect of pulse frequency on the weld pool dimensions, this parameter was changed according to Table

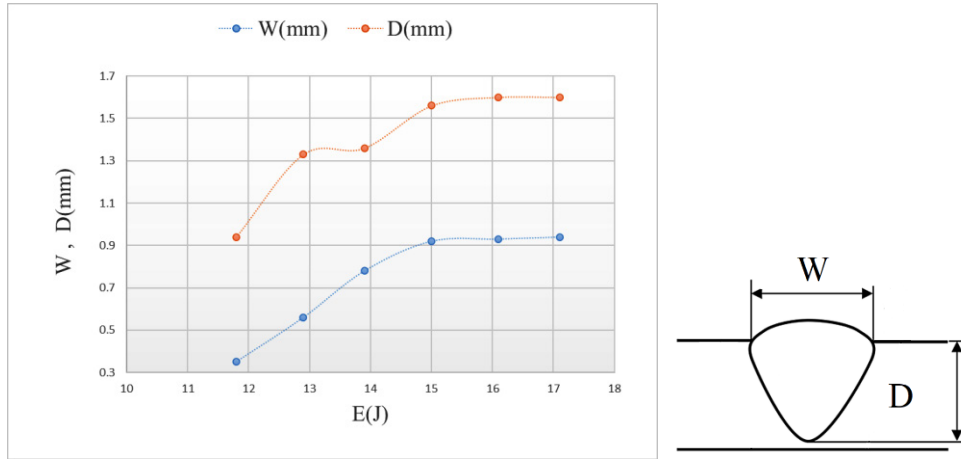


Fig. 12. The effect of pulse energy on weld pool dimensions in the dissimilar joint

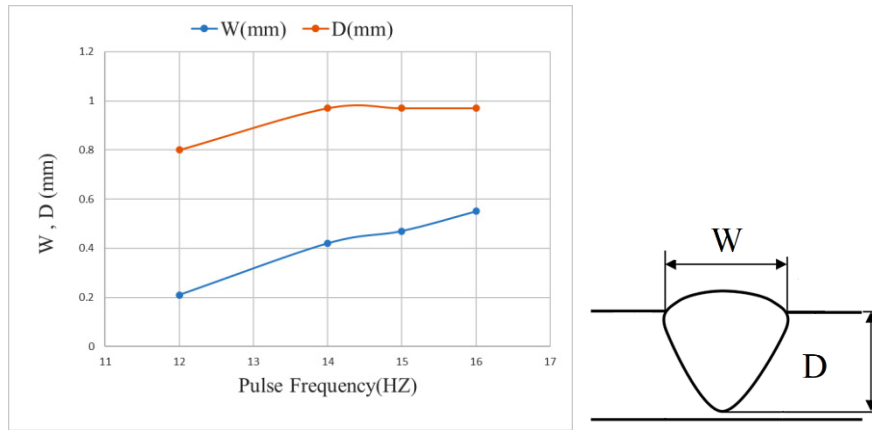


Fig. 13. The variations in weld dimensions with the pulse frequency in the similar joint of low-carbon steel sheets

2. Generally, as the frequency is increased at a constant pulse time, the average laser power increases, resulting in bigger weld pool dimensions. On the other hand, Concerning Eq. 4, which shows the overlap of the pulses, as the frequency is increased, the rate of pulse overlap is increased.

$$\%overlapping = \left(\frac{D - \frac{V}{f}}{D} \right) \times 100 \quad (4)$$

where V is welding speed, f is pulse repetition frequency and D is laser beam diameter [11].

Consequently, the zone where the subsequent pulse is to be placed on is somewhat pre-heated by the current pulse. The

preheating process increases the size of the melted zone. Fig. 13 illustrates the variations of weld pool dimensions in the similar joint of low-carbon steel with pulse frequency. The optimal pulse frequency was obtained in the experimental mode to be 14 Hz, which is consistent with the simulation results. As is evident, with the increase in the pulse frequency from 12 Hz to 14 Hz, the depth and width of the weld pool begin to increase with the same slope. Beyond the frequency of 14 Hz, the weld depth reaches a plateau, but the weld width increases more rapidly. Consequently, the depth/width ratio is decreased, deviating from the keyhole mode and the optimal state of welding. Thus, the optimal frequency for this joint will be 14 Hz.

Fig. 14 shows the variations in weld pool dimensions of the similar joint of stainless-steel plates with frequency. As can be seen, the weld width and depth increase with the increase in the pulse frequency, which was already explained

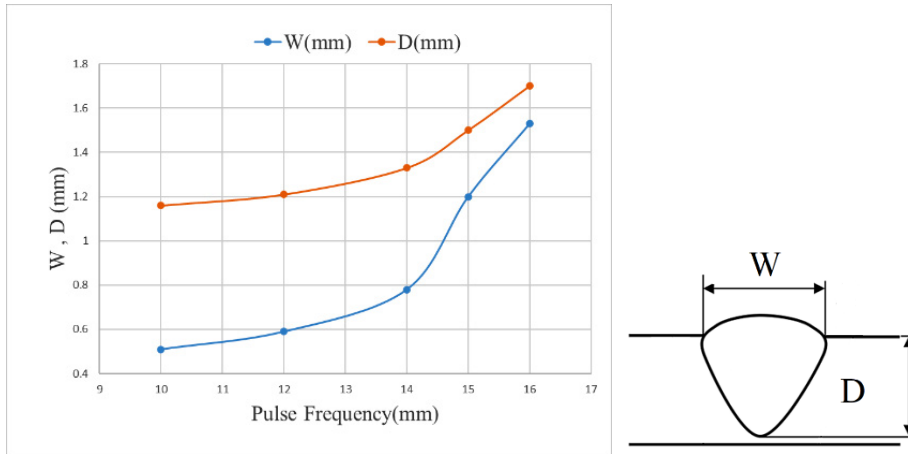


Fig. 14. The variations in weld pool dimensions with the pulse frequency in the similar joint of stainless-steel sheets

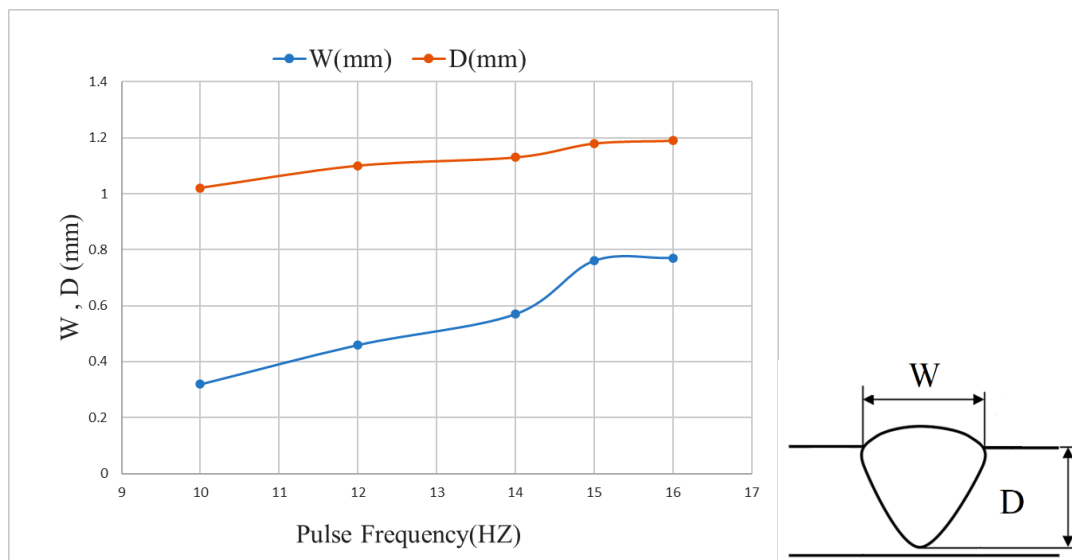


Fig. 15. The variations in weld pool dimensions with the pulse frequency in the dissimilar joint of stainless steel to low-carbon steel

in the previous section. Here, as the pulse frequency is changed from 10 Hz to 14 Hz, the percentage increase in the weld width and depth is constant. Then, with a further increase in the pulse frequency to over 14 Hz, the welding depth is increased by 20% but the welding depth by 9%. As a result, the depth/width ratio of the weld is decreased and the welding deviates from the optimal state. Accordingly, it can be concluded that the optimal frequency for this joint will be 14 Hz.

Fig. 15 shows the variations in weld dimensions of the dissimilar joint between stainless steel and low-carbon steel with the changes in the pulse frequency. As the pulse frequency changes, the weld width increases to a greater extent than the weld depth. This increase suddenly becomes more pronounced in the frequency shift from 14 Hz to 15 Hz, which reduces the width/depth ratio. Therefore, the 14 Hz

pulse frequency can be considered as the optimal frequency.

4- Conclusions

The present study used the finite element method to predict the shape of the weld pool and the effect of welding parameters on weld dimensions in the welding of low-carbon steel to stainless steel, low-carbon steel to low-carbon steel, and stainless steel to stainless steel. The main results can be summarized as below:

The size of the HAZ in laser welding is low due to the high-power density heat source and high cooling rate so its highest value is 115 μm , which happened in a similar joint of stainless steel. In the similar joint of low-carbon steel and dissimilar joint of stainless steel to low-carbon steel, the HAZ size is 90 and 75 μm , respectively.

The increase in the pulse energy enlarges the weld pool

and shifts it from conductive mode to the keyhole mode so that the keyhole mode happens at the pulse energy of 11.8, 13.9, and 17.1 J for the similar joint of stainless steel, similar joint of low-carbon steel, and their dissimilar joint, respectively.

The increase in the pulse frequencies increases their overlap, causing the preheating of the spots that have not met the heat source yet. As a result, the dimensions of the weld pool grow and deviate from the ideal keyhole state.

In all joints performed here, the width/depth ratio of the weld pool was found to be <1 at a pulse frequency of 14 Hz, and this is the optimal condition for the formation of the keyhole.

References

- [1] R. Blondeau, Metallurgy and mechanics of welding: processes and industrial applications, John Wiley & Sons, 2013.
- [2] M. Torkamany, M. Hamed, F. Malek, J. Sabbaghzadeh, The effect of process parameters on keyhole welding with a 400 W Nd: YAG pulsed laser, Journal of Physics D: Applied Physics, 39(21) (2006) 4563-4567.
- [3] D. Rosenthal, The theory of moving sources of heat and its application of metal treatments, Transactions of ASME, 68 (1946) 849-866.
- [4] M. Frewin, D. Scott, Finite element model of pulsed laser welding, WELDING JOURNAL, 78 (1999) 15-s-22-s.
- [5] A. Mahrle, J. Schmidt, The influence of fluid flow phenomena on the laser beam welding process, International Journal of heat and fluid flow, 23(3) (2002) 288-297.
- [6] S. Tsirkas, P. Papanikos, T. Kermanidis, Numerical simulation of the laser welding process in butt-joint specimens, Journal of materials processing technology, 134(1) (2003) 59-69.
- [7] M. Sunar, B. Yilbas, K. Boran, Thermal and stress analysis of a sheet metal in welding, Journal of Materials Processing Technology, 172(1) (2006) 123-129.
- [8] J. Sabbaghzadeh, M. Azizi, M.J. Torkamany, Numerical and experimental investigation of seam welding with a pulsed laser, Optics & Laser Technology, 40(2) (2008) 289-296.
- [9] B. Yilbas, A. Arif, B.A. Aleem, Laser welding of low carbon steel and thermal stress analysis, Optics & Laser Technology, 42(5) (2010) 760-768.
- [10] K. Balasubramanian, N.S. Shanmugam, G. Buvanashakaran, K. Sankaranarayanan, Numerical and experimental investigation of laser beam welding of AISI 304 stainless steel sheet, Advances in Production Engineering & Management, 3(2) (2008) 93-105.
- [11] N.S. Shanmugam, G. Buvanashakaran, K. Sankaranarayanan, Some studies on weld bead geometries for laser spot welding process using finite element analysis, Materials & Design, 34 (2012) 412-426.
- [12] J. Wilson, J.F.B. Hawkes, Lasers : principles and applications, Prentice Hall, New York, 1987.
- [13] E. Assuncao, S. Williams, Comparison of continuous wave and pulsed wave laser welding effects, Optics and lasers in Engineering, 51(6) (2013) 674-680.
- [14] K. Kim, J. Lee, H. Cho, Analysis of pulsed Nd: YAG laser welding of AISI 304 steel, Journal of Mechanical Science and Technology, 24(11) (2010) 2253-2259.
- [15] Z. Sun, J. Ion, Laser welding of dissimilar metal combinations, Journal of Materials Science, 30(17) (1995) 4205-4214.
- [16] R.B. Jose, M.d.N. de Rossi Wagner, M. David, V.J. de Almeida Ivan Alves, N. Dias, Pulsed Nd: YAG laser welding of AISI 304 to AISI 420 stainless steels, Opt Laser Eng, 45 (2007) 960-966.
- [17] M. Jafarzadegan, A. Abdollah-Zadeh, A. Feng, T. Saeid, J. Shen, H. Assadi, Microstructure and mechanical properties of a dissimilar friction stir weld between austenitic stainless steel and low carbon steel, Journal of Materials Science & Technology, 29(4) (2013) 367-372.
- [18] A. Mackwood, R. Crafer, Thermal modelling of laser welding and related processes: a literature review, Optics & Laser Technology, 37(2) (2005) 99-115.
- [19] E. Anawa, A. Olabi, Using Taguchi method to optimize welding pool of dissimilar laser-welded components, Optics & Laser Technology, 40(2) (2008) 379-388.
- [20] M. Jiang, N. Jiang, X. Chen, S. Ma, Y. Chen, Y. Chen, Z. Lei, Experimental and numerical investigation of single-pass laser welding of 20 mm-thick high-strength steel under reduced ambient pressure, Journal of Materials Research and Technology, 15 (2021) 2317-2331.
- [21] S. Yan, Z. Meng, C. Tan, X. Song, G. Wang, Prediction of temperature field and residual stress of oscillation laser welding of 316LN stainless steel, Optics & Laser Technology, 145 (2022).
- [22] A.K. Unni, V. Muthukumar, Modeling of heat transfer, fluid flow, and weld pool dynamics during keyhole laser welding of 316 LN stainless steel using hybrid conical-cylindrical heat source, (2022).
- [23] M. Masoumi, A study on the structure, mechanical strength and failure behavior of laser spot welds of carbon steel sheets, Amirkabir University of Technology, 2010.
- [24] X. Zhu, Y. Chao, Numerical simulation of transient temperature and residual stresses in friction stir welding of 304L stainless steel, Journal of materials processing technology, 146(2) (2004) 263-272.
- [25] S. Bag, A. Trivedi, A. De, Development of a finite element based heat transfer model for conduction mode laser spot welding process using an adaptive volumetric heat source, International Journal of Thermal Sciences, 48(10) (2009) 1923-1931.
- [26] W. Chang, S.-J. Na, A study on the prediction of the laser weld shape with varying heat source equations and the thermal distortion of a small structure in micro-joining, Journal of materials processing technology,

- 120(1-3) (2002) 208-214.
- [27] B. Tam, M. Khan, Y. Zhou, Mechanical and functional properties of laser-welded Ti-55.8 Wt Pct Ni nitinol wires, *Metallurgical and Materials Transactions A*, 42(8) (2011) 2166-2175.
- [28] J.R. Chukkan, M. Vasudevan, S. Muthukumaran, R.R. Kumar, N. Chandrasekhar, Simulation of laser butt welding of AISI 316L stainless steel sheet using various heat sources and experimental validation, *Journal of Materials Processing Technology*, 219 (2015) 48-59.
- [29] X. Shen, W. Liu, S. Lei, Three-dimensional thermal analysis for laser assisted milling of silicon nitride ceramics using FEA, in: *ASME International Mechanical Engineering Congress and Exposition*, 2005, pp. 445-452.

HOW TO CITE THIS ARTICLE

Z. Tajbakhshjoo, E. RanjbarNodeh, A. Farzadi, E. Family, *Finite element modeling of heat transfer in pulsed laser welding of similar and dissimilar carbon and stainless steels*, *AUT J. Mech Eng.*, 7(2) (2023) 117-130.

DOI: [10.22060/ajme.2023.21838.6047](https://doi.org/10.22060/ajme.2023.21838.6047)



